Acta Pharmaceutica Sinica B 2019;9(4):843–857

Chinese Pharmaceutical Association
Institute of Materia Medica, Chinese Academy of Medical Sciences

Acta Pharmaceutica Sinica B

www.elsevier.com/locate/apsb
www.sciencedirect.com

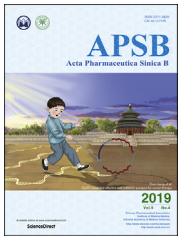

ORIGINAL ARTICLE

Menthol-modified casein nanoparticles loading 10-hydroxycamptothecin for glioma targeting therapy

Caifang Gao[a,b], Jianming Liang[a,c], Ying Zhu[c], Chengli Ling[d], Zhekang Cheng[e], Ruixiang Li[a], Jing Qin[a], Weigen Lu[b,*], Jianxin Wang[a,*]

[a]*Department of Pharmaceutics, School of Pharmacy, Fudan University & Key Laboratory of Smart Drug Delivery, Ministry of Education, Shanghai 201203, China*
[b]*Shanghai Institute of Pharmaceutical Industry, China State Institute of Pharmaceutical Industry, Shanghai 201203, China*
[c]*Guangzhou University of Chinese Medicine, Guangzhou 510006, China*
[d]*School of Pharmacy, Chengdu University of Traditional Chinese Medicine, Chengdu 611137, China*
[e]*School of Pharmacy, Minzu University of China, Beijing 100081, China*

Received 13 October 2018; received in revised form 22 November 2018; accepted 18 December 2018

KEY WORDS

Glioma;
Casein;
Menthol;
Nanoparticles;
Brain targeting;
Blood–brain barrier;
10-Hydroxycamptothecin

Abstract Chemotherapy outcomes for the treatment of glioma remains unsatisfactory due to the inefficient drug transport across the blood–brain barrier (BBB) and insufficient drug accumulation in the tumor region. Although many approaches, including various nanosystems, have been developed to promote the distribution of chemotherapeutics in the brain tumor, the delivery efficiency and the possible damage to the normal brain function still greatly restrict the clinical application of the nanocarriers. Therefore, it is urgent and necessary to discover more safe and effective BBB penetration and glioma-targeting strategies. In the present study, menthol, one of the strongest BBB penetration enhancers screened from traditional Chinese medicine, was conjugated to casein, a natural food protein with brain targeting capability. Then the conjugate self-assembled into the nanoparticles to load anti-cancer drugs. The nanoparticles were characterized to have appropriate size, spheroid shape and high loading drug capacity. Tumor spheroid penetration experiments demonstrated that penetration ability of menthol-modified casein nanoparticles (M-CA-NP) into the tumor were much deeper than that of unmodified nanoparticles. *In vivo* imaging further verified that M-CA-NPs exhibited higher brain tumor distribution than unmodified nanoparticles. The median survival time of glioma-bearing mice treated with HCPT-M-CA-NPs was significantly prolonged than those treated with free HCPT or HCPT-CA-NPs. HE staining of

*Corresponding authors. Fax: +86 21 51980087.
E-mail addresses: sipiluwg@163.com (Weigen Lu), jxwang@fudan.edu.cn (Jianxin Wang).

Peer review under responsibility of Institute of Materia Medica, Chinese Academy of Medical Sciences and Chinese Pharmaceutical Association.

https://doi.org/10.1016/j.apsb.2019.01.006

the organs indicated the safety of the nanoparticles. Therefore, the study combined the advantages of traditional Chinese medicine strategy with modern delivery technology for brain targeting, and provide a safe and effective approach for glioma therapy.

1. Introduction

Glioma is the most common intracranial malignancy in the central nervous system (CNS)[1]. According to the statistics of the central brain tumor registry of the United States (CBTRUS), glioma accounts for 27% of all central nervous system tumors, about 80% of which is malignant tumor. Among the primary malignant CNS tumors, the incidence of glioma is the highest, accounting for 46.1%[2]. The treatment of glioma is based on surgical resection of tumors, combined with radiotherapy and chemotherapy[3]. However, due to the infiltrative growth of glioma, the boundaries between tumor tissue and normal brain tissue are very blurred. To avoid the damage to the brain function, it is hard to remove all tumors by surgical treatment, resulting in very poor prognosis and easy relapse[4]. The clinical outcome of radiation therapy is also limited because it is difficult to control the scope of treatment accurately and will cause normal brain tissue damage[5]. Therefore, chemotherapy still occupies an important position in the treatment of glioma[6,7].

However, the presence of the blood–brain barrier (BBB), which is mainly composed of polarized brain capillary endothelial cells through complex intercellular tight junctions, creates a relatively stable internal environment that safeguards the normal physiological functions of CNS, but greatly limits the efficiency of chemotherapeutic drugs into the brain[1,8,9]. About 98% of small molecule chemical drugs and almost 100% of macromolecular drugs are difficult to enter the brain, which has brought great difficulties to the treatment of brain tumors[10]. Based on the transport of the substance across the BBB, researchers have developed many strategies for enhancing brain-targeted delivery of drugs: (1) prodrugs with good fat-solubility; (2) receptors, transporters, and adsorptive-mediated modalities to achieve trans-brain barrier transport; (3) BBB disruption techniques[11,12]. Apart from BBB, the blood–brain tumor barrier (BBTB) and complex tumor environment (TME) characteristics further limit the treatment of glioma. Therefore, dual-targeting systems, which can overcome multiple delivery barriers, have been developed rapidly and proved to be an effective strategy for brain tumors[13,14]. For example, angiopep-2-decorated gold nanoparticle was designed to delivery doxorubicin to glioma through an acid-responsive linker. The anti-glioma results indicated that the system can significantly prolong the median survival time of glioma-bearing mice[15]. Menthol is a natural cyclic monoterpene alcohol from plant mint, and has been widely used in oral hygiene products, cosmetics, medicines, etc.[16].

According to the reports, menthol can increase the distribution of drugs in the brain, enhance the transdermal absorption of drugs, raise the efficiency of gene transfection, and can guide the drug to reach the target site for improving the efficacy[17–21]. In addition, it can enhance the penetration of drugs to cross a variety of physiological barriers, such as BBB, gastrointestinal mucosa barrier and skin[22]. For example, menthol can promote puerarin transport across MDCK and MDCK–MDR1 cells as *in vitro* BBB model[23]. In our previous study, we found that co-incubation of borneol (an aromatic resuscitation compound) with nanoparticles can increase the uptake of nanoparticles in human brain capillary endothelial cells (BCECs) and significantly increase the accumulation of nanoparticles in the brain[24]. Ren et al.[25] prepared borneol-modified acyclovir solid lipid nanoparticles and found that the distribution of acyclovir in the brain was significantly enhanced. Since both menthol and borneol have been applied as messenger drugs in traditional Chinese medicine, it could be deduced that menthol has the potential to improve the transport of nanoparticles into the brain. Although the co-incubation of menthol and borneol with drugs or nanoparticles could improve their BBB transportation, the effect was limited and uncontrollable, since the drug and the enhancer usually cannot arrive at the BBB simultaneously. Therefore, the modification of enhancers onto nanoparticles has been utilized to improve their permeation capability through various barriers. The conjugation of borneol, muscone and menthol with bovine serum albumin (BSA) nanoparticles could effectively enhance the brain accumulation of nanoparticles[26]. The modification of borneol on the surface of solid lipid nanoparticles (bSLPs) could enhance their transport through the BBB, compared with the unmodified SLPs[27]. The BBB penetration improvement of nanoparticles by the modification of natural permeation enhancers could be attributed to increased lipophilicity and endocytosis, downregulated TJs-associated proteins levels, such as ZO-1 and occludin protein, and bypassing the BBB *via* pineal pathway[26].

Besides the targeting ligands, carriers also play an important role in drug delivery. The carriers for preparing nanoparticles include synthetic high molecular polymers, such as PLA, PLGA, PCL, PAMAM, etc., and natural polymer materials, such as proteins and polysaccharides[28–31]. Compared with synthetic polymers, natural materials have many unique properties, for example, they are generally safer and can enclose both hydrophobic drugs and hydrophilic drugs. The use of natural macromolecules to construct drug carriers by simple and easy green chemistry can effectively avoid the use of synthetic chemical reagents and organic solvents, which is very beneficial to their application in biopharmaceutical industry[32]. In addition, functional groups, such as disulfide bonds, amino groups and carboxyl groups, exist in the structure of the proteins themselves, so they can be modified with many targeting ligands on the surface[33]. Although two albumin-based particulate formulations have been approved for clinical use, the utilization of native proteins in terms of particulate drug delivery systems is still limited by their relatively poor tumor penetration and insufficient source of albumin[34,35]. Therefore, more handy and cheap proteins have been sought to replace albumin for the development of tumor targeting drug delivery systems.

Casein (CA) is the main component of milk and consists of four components: αs_1-, αs_2-, β- and κ-casein. The mass ratio of them in

milk is approximately 3:0.8:3:1 and the molecular weight range is 19–25 kD[36,37]. They are all chain-like amphiphilic proteins with no definite structure. As a natural food protein, casein has the characteristics of wide source, low price, safety, non-toxic and high nutritional value[38]. In recent years, a variety of casein delivery systems have been developed and reported. As an ideal carrier, the hollow casein nanospheres have extraordinary ability to penetrate cell membranes, regardless of cell type and temperature. The uptake of casein is non-endocytosis and would not induce cell damage and cytotoxicity[39,40]. The cell membrane permeability of CA was similar to that of cell-penetrating peptides (CPPs), a powerful transport vector tool. However, CPPs need to be conjugated with cargoes, thereby holding the risk to alter the biological activity of cargoes. Thus, the development of nanoscale carriers which can penetrate cell membranes by themselves in a non-classical fashion is highly desirable. It has been found that the cisplatin-encapsulated casein nanoparticles have strong ability to accumulate in tumor site, deliver cisplatin into the deep part of the tumor, penetrate the cell membrane barrier, and finally inhibit the growth of tumor significantly[41]. Therefore, CA was regarded as a natural, efficient, cheap and easily-handled tumor-targeting drug carrier.

10-Hydroxycamptothecin is the most effective alkaloid in the same type of anti-tumor monomers extracted from Chinese *Camptotheca* acuminate in 1960s and 1970s[42]. As an anti-tumor drug with broad spectrum, it is a cell cycle specific drug and mainly acts on DNA synthesis[43]. However, the clinical application of the drug was restricted by its short half life (about 30 min), poor water-solubility, and lactone ring sensitivity to light and pH[44]. Therefore, it is necessary to develop its new dosage forms to overcome the above problems.

In this study, a novel nanoparticle system was developed by taking casein as carrier and modified with menthol as brain-targeting ligand. By combining the advantages of natural aromatic resuscitation component and food protein, the system can provide efficient and safe brain tumor targeting ability and improve the treatment effect of 10-hydroxycamptothecin.

2. Materials and methods

2.1. Materials and reagents

Caseinate, 4′,6-diamidino-2-phenylindole (DAPI), (4,5-dimethylthiazol-2-yl)-2,5-diphenyl tetrazolium bromide (MTT) and propidium iodide (PI) were purchased from Sigma–Aldrich (St. Louis, MO, USA). *Para*-mentha-8-thiolone, 2-iminothiolane hydrochloride, 1,4-butanediol diglycidyl ether and 5,5′-dithiobis-(2-nitrobenzoic acid) (DTNB) were purchased from J&K Chemical Ltd. (Shanghai, China). Trinitrobenzene sulphonic acid (TNBS) was from Thermo Fisher Scientific Co. (USA). 10-Hydroxy camptothecin was purchased from Meilune Biological Technology Co., Ltd. (Dalian, China). 1,1′-Dioctadecyl-3,3,3′,3′-tetramethylindodicarbocyanine perchlorate (DiD) and 1,1′-dioctadecyl-3,3,3′,3′-tetramethylindotricarbocyanine iodide (DiR) were from Beijing Fanbo Science and Technology Co., Ltd. (Beijing, China). BSA and coumarin 6 (Cou-6) were from Aladdin Corp. (Shanghai, China). All the other chemicals were analytical reagent grades and purchased from Sinopharm Chemical Reagent (Shanghai, China).

2.2. Cells and animals

Brain capillary endothelial cells (BCEC) and glioblastoma cells (C6) were obtained from Cell Bank, Chinese Academy of Sciences (Shanghai, China). The cells were cultured in Dulbecco's Modified Eagle's Medium (DMEM) supplemented with 10% FBS, 1% L-glutamine, 1% nonessential amino acids, 100 U/mL penicillin and 100 μg/mL streptomycin at 37 °C under a humidified atmosphere containing 5% CO_2.

BALB/c nude mice (male, 4–5 weeks, 18–22 g) were obtained from Shanghai Laboratory Animal Research Center (Shanghai, China) and maintained under standard housing conditions. All animal experiments were carried out in accordance with the protocols evaluated and approved by the ethics committee of Fudan University (Shanghai, China).

2.3. Synthesis and characterization of menthol-modified casein

Menthol-modified casein was synthesized following the steps below. Firstly, 2-iminothiolane hydrochloride was grafted to casein as 30:1 (mol/mol) in sodium carbonate buffer by incubating for 30 min at ambient temperature to form thiolated casein. Then, 1,4-butanediol diglycidyl ether ethanol was added to the above reaction solution, continuing to incubate for 4 h. After that, the product was applied to sephadex LH-20 column to remove the unconjugated reactants. Subsequently, *para*-mentha-8-thiolone ethanol solution was mixed with the above purified product and then stirred for 24 h at room temperature. The end-product was added with 10-fold volume ethanol-ethyl acetate solution (1:1, *v/v*) and centrifuged for 45 min at 3821 × *g* (Xiangyi high speed refrigerated centrifuge, Hunan, China) at 4 °C. Finally, the harvested precipitate re-dissolving in ultrapure water was dialysed for 4 h in distilled water and filtered through a 0.22 μm syringe filter to obtain the targeting product menthol-modified casein (M-CA).

To confirm the successful conjugation of M-CA, the retention time in HPLC was observed and the change of the molecule weight after modification was viewed by SDS-PAGE electrophoresis.

2.4. Preparation and characterization of NPs

HCPT-M-CA-NPs and HCPT-CA-NPs were prepared as reported with minor modification[45,46]. A 40 mg/mL stock solution of HCPT in dimethyl sulfoxide (DMSO) was freshly prepared prior to use. A stock solution of caseinate was prepared by dissolving 10 mg/mL casein in 0.1 mol/L phosphate-buffered saline (PBS). Then 25 μL DMSO containing 1 mg HCPT was added to 1 mL caseinate PBS solution slowly. When the mixed solution was homogeneous, it was ultrasonated in ice-bath at proper power and time (200 W, 5 min). Then, the suspension was centrifuged to remove the free HCPT and DMSO, and the residues were collected as nanoparticles.

The size distribution and zeta potential of nanoparticles were measured by dynamic light scattering (DLS, Zetasizer Nano ZS, Malvern, UK). The morphology of NPs was detected by transmission electron microscope after negative staining with 1% uranyl acetate solution. To determine the encapsulation efficiency (EE) and drug-loading capacity (DLC), the prepared nanoparticles was passed through/or not 0.22 μm syringe filter, treated with methanol 1:10 (*v/v*) at ambient temperature for 10 min to completely extract HCPT. The concentration of HCPT encapsulated into nanoparticle and total input was acquired on a high performance liquid chromatography (Agilent) with a UV detector set at 383 nm. The EE and DLC were calculated as previously described[47].

2.5. Stability of NPs

To assess the stability of the nanoparticles, the particle size and zeta potential were measured using DLS in 4 °C at Days 0–7. The changes were drawn with Graphpad Prism 7 (GraphPad Software, Inc., La Jolla, USA).

2.6. In vitro release profiles

The HCPT release behavior from the NPs was performed by using a dialysis method. Briefly, 1 mL nanoparticle suspension containing 50 μg/mL HCPT was sealed into a dialysis bag. Then the bag was immersed into 100 mL PBS containing 1% SDS to meet the sink condition. The experiment was conducted at 37 °C with continuous stirring at 100 rpm (Desktop full temperature oscillator: Taicang Experimental Equipment Factory, Suzhou, China). At predetermined time intervals, 1 mL of the release medium was withdrawn for measurement and replenished with an equal volume of fresh medium. The released amount of HCPT was determined by fluorescence spectrophotometry (Agilent, USA).

2.7. Cellular uptake

To evaluate the uptake efficiency of different formulations qualitatively, BCEC and C6 cells were seeded into 6-well plate at a density of 5×10^4 /well. BSA, casein and menthol modified casein nanoparticles encapsulating Cou-6 were prepared, respectively. After incubated for 24 h, the cells were treated with 1 mL different formulations containing 50 ng/mL Cou-6, incubated at 37 °C for 4 h, stained with Hoechst 33342 and then washed with cold PBS buffer three times. After that, the cells were added 300 μL PBS and photographed by fluorescence microscopy (LEICA, Germany).

To assess the uptake efficiency of different formulations quantitatively, BCEC and C6 cells were seeded into 12-well plate at a density of 1×10^5 /well. When the cells achieved 80% confluence, the medium was replaced with different protein-based NPs described above and incubated for 4 h. After the incubation, the cells were washed with PBS buffer and collected after digestion, subjected to centrifugation at 2500 rpm (H1850R desktop high speed refrigerated centrifuge: Xiangyi Experimental Instrument Development Co., Ltd., Hunan, China) for 5 min and analyzed using a flow cytometer (FACS Calibur, BD, USA).

2.8. Penetration in glioma spheroids of NPs

The penetration depth inside the tumor spheroids of different formulations was detected by confocal microscopy (Zeiss, Germany). C6 cells were seeded at a density of 2×10^3 cells/well in 96-well plates coated with 50 μL of 2% (*w/v*) agarose gel, cultured at 37 °C, 5% CO_2 for 7 days to form the 3D tumor spheroids[48]. The tumor spheroids were cultured with the NPs loaded with DiD for 12 h and subjected to confocal microscopy after being washed with PBS three times.

2.9. In vitro cytotoxicity

The cytotoxicity of different casein formulations on C6 cells was assessed by MTT assay ($n = 6$). In brief, the cells were seeded at a density of 1×10^4/well in 96-well plate and incubated at 37 °C, 5% CO_2 for 24 h. HCPT-loaded casein nanoparticles were diluted into gradient concentration with complete medium and then added to the wells. After incubation for 48 h, the medium were discarded and 20 μL MTT solution (5 mg/mL) was added to each well. Four hours later, the MTT solution was replaced with 100 μL DMSO and shaken for 10 min at 37 °C. Finally, the 96-well plates were scanned *via* a microplate reader and the absorbance was measured at 490 nm.

2.10. In vitro cell apoptosis

The apoptosis of C6 cells was qualitatively visualized and quantitatively measured using fluorescence microscopy and fluorescence-activated cell sorting. The cells were seeded at a density of 1×10^5/well in 6-well plate and allowed to grow for 24 h. The cultured medium was then substituted with CA-NPs and M-CA-NPs (equal to 312 ng/mL of HCPT) with subsequent 48 h incubation. After being washed with cold PBS, the cells were stained with PI, Hoechst 33342 and DAPI, then subjected to fluorescence microscopy to capture images. In addition, the collected cells were washed again with PBS three times and stained with an annexin V-FITC apoptosis detection kit according to the manufacturer's protocol. The cells were subjected to apoptosis analysis using FACS.

2.11. Animal model establishment

To establish the *in situ* glioma model, the nude mice were anaesthetized by 1% pentobarbital sodium and C6 cells (5×10^5 cells/5 μL) were injected into the nude at striatum, 2 mm right lateral to the bregma and 4 mm of depth.

2.12. In vivo imaging

Twelve days after inoculation C6 cells, the glioma-bearing nude mice were randomly divided into 3 groups ($n = 3$) and were injected 200 μL formulations loaded DiR through tail vein. At the predetermined time point, the distribution of fluorescence in mice was observed using an *in vivo* Imaging System (IVIS, Caliper, Newton, MA, USA). After 24 h, the mice were anesthetized and subjected to cardiac perfusion using 4% paraformaldehyde and PBS buffer, and then the brain and other main organs were excised for further imaging by IVIS.

2.13. In vivo anti-glioma effect

The orthotopic glioma-bearing mice were established as described above. Seven days after the inoculation, the mice were randomly divided into 4 groups ($n = 10$), saline, free HCPT, HCPT-CA-NPs and HCPT-M-CA-NPs. Each mouse was administrated at a dose of 5 mg/kg HCPT respectively, at Days 7, 9, 12, 15, 18 and 21 through tail intravenous injection. The body weight of the mice was measured every other day. The efficacy was judged according to the median survival time after treatment.

2.14. Histopathological examination

At the experimental end point, major organs were collected for histopathological examination to assess the safety of various formulations.

2.15. Binding affinity of casein with LDL receptors

The structure of casein is similar with that of low density lipid (LDL) protein. It has been proved that LDL receptors are highly expressed in BCEC and C6 cells[49]. We surmised that casein nanoparticles might be transported into the cells through the interaction with LDL receptors, and resulted in dual targeting. Thus, the binding assay was conducted to study the mechanisms that casein can promote cellular uptake and penetrate into the tumor cells.

BCEC cells were seeded into 6-wells plates at a density of 5×10^4 cells per well and incubated at 37 °C for 24 h. Afterwards, the cells were treated with fresh medium containing proper amount of rhodamine-casein and rhodamine-menthol-casein for 1 h. Then the cells were washed, fixed and incubated with primary antibodies and a secondary antibody, and then examined using laser confocal fluorescence microscopy.

2.16. Effect on the expression ZO-1 and occludin

To evaluate the expression of the ZO-1 and occludin, BCEC cells were seeded into 6-well culture-plates with a density of 5×10^5 cells per well and incubated at 37 °C for five days. Then the BCEC monolayer was treated with casein and menthol-modified casein. After 4 h, the cells were collected and lysed using RPMI buffer containing 1 mmol/L PMSF. The protein concentration was determined by BCA method. Equivalent amount of proteins was boiled for 5 min in loading buffer, separated by SDS-polyacrylamide gel electrophoresis, and then transferred to nitrocellulose membranes. After blocked for 1 h in TBS containing 5% milk albumin, the membranes were then probed with the specific antibodies recognizing the target proteins and the proteins were visualized using an ECL reagent.

2.17. Statistical analysis

Data were presented as mean ± SD. Statistical differences in cellular uptake, cell apoptosis, *in vivo* imaging were determined by Student's *t*-test. The probability of survival was determined by Kaplane–Meier method and compared by log-rank test. P value < 0.05 was considered statistically significant.

3. Results and discussions

3.1. Synthesis and characterization of menthol-modified casein

The structures of chemicals and synthetic schemes of modified casein were shown in Scheme 1. The main active component of peppermint is menthol, but it is hard for menthol to couple with casein. So *para*-mentha-8-thiolone was used as a menthol analog. 2-Iminothiolane reacted firstly with the amino residues of casein to introduce sulfhydryl groups. Then 1,4-butanediol diglycidyl ether, as an intermediate linker, linked with thiolated casein and menthone through an alkaline ring-opening reaction. The modification rate of M-CA was 87.6 ± 3.5%. As shown in Supporting Information Fig. S1A, four clear bands were observed at 19–25 kD in casein group (lanes 1, 2 and 3), and the menthol-modified casein bands (lanes 4 and 5) were above the casein band and the bands after modification became one band. The result confirmed the success of protein modification. HPLC chromatogram and retention time were shown in Fig. S1B and C. The change of retention time also indicated successful menthol modification and the result was in accordance with that of the SDS-PAGE gel. The four bands and peaks became one after modification. Thus, we surmised that there was one casein component which was easy to modify and other three components might be removed during the synthesis process.

3.2. Preparation and characterization of NPs

Chemical cross-linking is a critical method applied for stabilization of casein nanoparticles, which, however, usually involves the use of toxic cross-linking agents (*e.g.*, glutaraldehyde). In this work, we developed a green method based on the amphiphilic structure of casein and drug-induced self-assembly for casein nanoparticle preparation. Simple mixture and ultrasound operation could successfully prepare nanoparticles and almost has no organic solvent. The particle sizes of HCPT-CA-NPs and HCPT-M-CA-NPs were 125.4 ± 0.71 and 131.5 ± 0.92 nm, respectively. The particle sizes did not exhibit significant variations with the modification of menthol. Encapsulation of coumarin-6, DiD, and DiR did not affect the particle size (data not shown). The size distribution

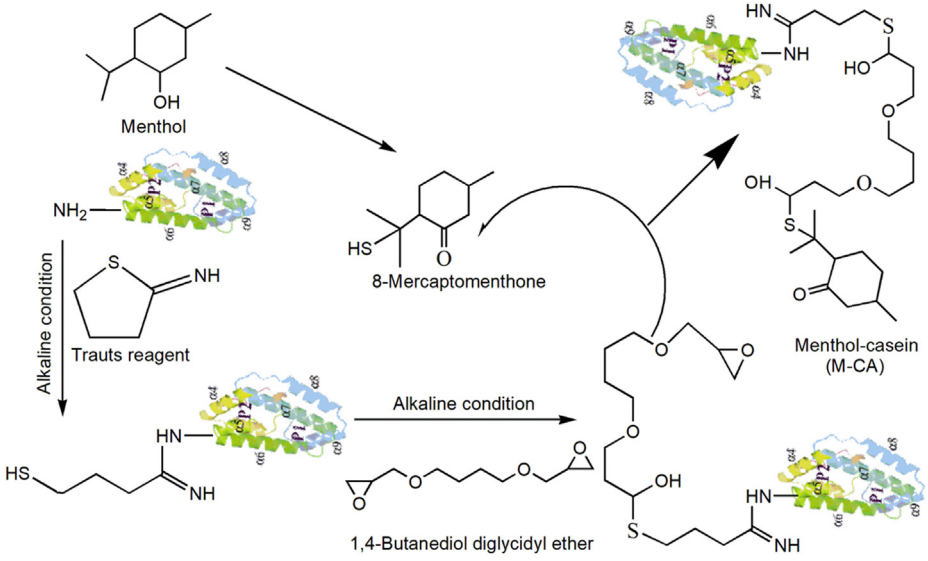

Scheme 1 The synthesis procedure of menthol-casein.

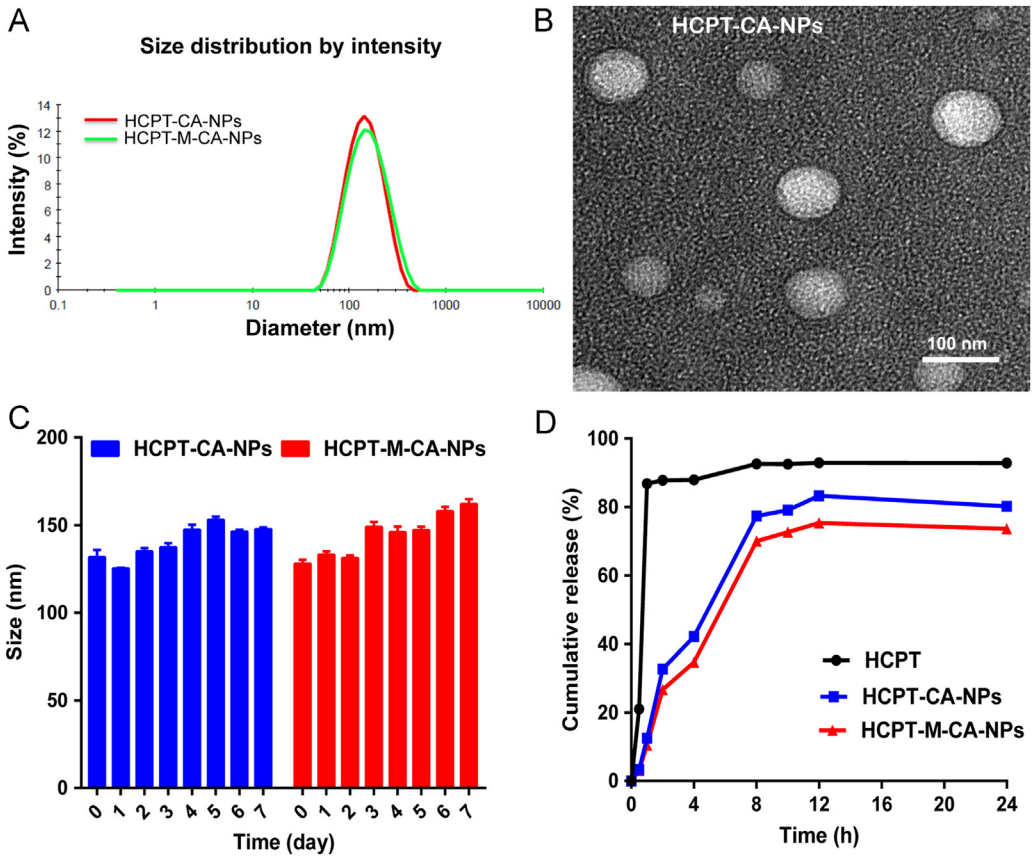

Figure 1 Characterization of the casein NPs. (A) Size of casein NPs. (B) TEM of casein NPs. (C) Stability of NPs at 4 °C. (D) *In vitro* release of 10-hydroxycamptothecin (HCPT). Data are expressed as mean ± SD, $n = 3$.

Table 1 Physical characterization of the HCPT-CA-NPs and HCPT-M-CA-NPs.

Nanoparticle	CA NP	M-CA NP
Particle mean size (nm)	125.4 ± 0.71	131.5 ± 0.92
PDI	0.18 ± 0.01	0.20 ± 0.01
Zeta potential (mV)	−28.57 ± 0.75	−30.26 ± 1.15
Encapsulation efficiency (%)	95.43 ± 1.29	93.76 ± 2.84
Drug loading capacity (%)	9.12 ± 0.58	8.64 ± 0.76

graphs of HCPT-CA-NPs and HCPT-M-CA-NPs are shown in Fig. 1A. The morphological observation by TEM image revealed that HCPT-CA-NPs were homogeneously spheroids (Fig. 1B). Zeta potentials were approximately −28.57 and −30.26 mV for HCPT-CA-NPs and HCPT-M-CA-NPs, respectively. The Zeta potentials were negative and changed slightly after the modification of menthol. The HCPT entrapment efficiencies of both nanoparticles were above 90%, and the drug-loading percent of HCPT in the nanoparticles was around 9%, indicating good entrapment efficiencies. The detailed physicochemical characteristics and loading parameters are listed in Table 1.

3.3. *The stability and release behavior of NPs*

The storage stability of nanoparticles at 4 °C was investigated using the change of particle size and zeta potential as indexes. As shown in Fig. 1C, no significant changes were observed in one-week study, implying that the nanoparticles can be well preserved at 4 °C without aggregation.

The release characteristics of HCPT from the nanoparticles were determined using the dialysis method and performed in PBS (0.01 mol/L, pH 7.4). As shown in Fig. 1D, compared with the rapid release (more than 80% within 1 h) of free HCPT, both HCPT-loaded nanoparticles exhibited sustained release profiles. Less than 60% HCPT was released from nanoparticles within 6 h, and no initial burst release was detected.

3.4. *In vitro cellular uptake of the NPs*

The cellular uptake of nanoparticles was examined on BCEC and C6 cell models. The uptake fluorescence intensity was qualitatively and quantitatively studied using inverted fluorescence

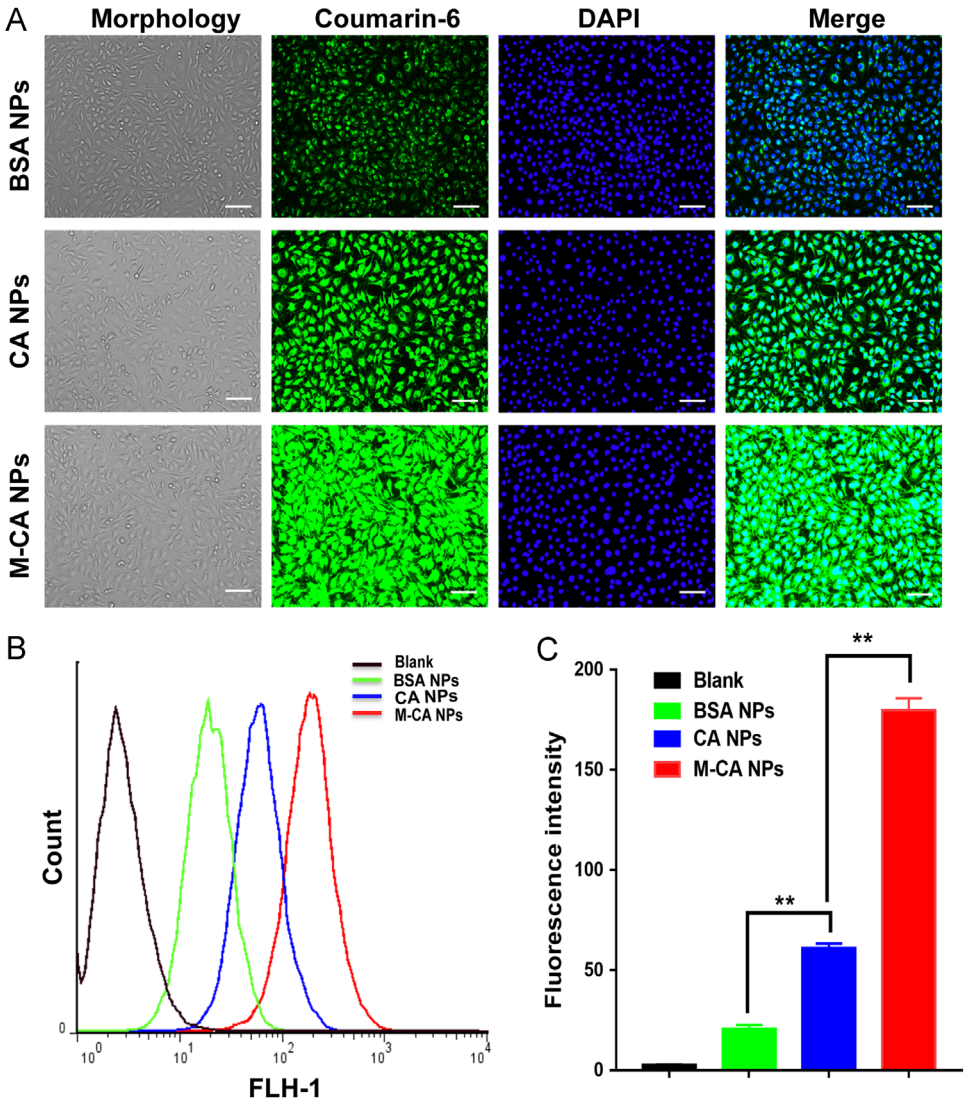

Figure 2 Cellular uptake of nanoparticles at equivalent C6 concentration (50 ng/mL) after incubation for 4 h at 37 °C on BCEC cells. (A) Representative fluorescence photomicrographs of BCEC cells after treatment with different coumarin-loaded nanoparticles (bar: 100 μm). (B) FACS analysis of the uptake and (C) the column chart of the median fluorescence intensity of different nanoparticles groups. Data are represented as mean ± SD, $n = 3$. $^{**}P < 0.05$.

microscopy and flow cytometry. As shown in Figs. 2A and 3A, compared with BSA NPs, the fluorescence intensity of CA NPs in BCEC and C6 cells was significantly enhanced, indicating that casein nanoparticles have stronger ability to penetrate cell membranes into the cells. Furthermore, the modification of menthol could further promote the uptake of CA NPs. The fluorescence signal in BCEC cells of M-CA NPs was stronger than that of CA NPs. As shown in Figs. 2B, C and 3B, C of FACS results, on BCEC cells, the uptake fluorescence intensity of CA NPs and M-CA NPs was 2.96- and 8.72-fold of that of BSA NPs, respectively. It is similar on C6 cells, with the uptake intensity of CA NPs and M-CA NPs being 3.02 and 6.47 times higher than that of BSA NPs, respectively. The results of qualitative fluorescence microscopy and the quantitative flow cytometry showed a consistent trend, indicating that casein has stronger ability to penetrate into the cells than albumin, and the modification of menthol could further enhance the ability of nanoparticles to diffuse into the cells.

3.5. *Penetration in tumor spheroids of NPs*

Poor drug intratumoral infiltration is a daunting obstacle against effective cancer therapy[50]. The penetrating ability of nanoparticles was evaluated *in vitro* in 3D tumor spheroids by using a C6 spheroid culture model and measured by confocal microscope. As shown in Fig. 4, M-CA NPs displayed extensive penetration inside the spheroids and penetrated significantly deeper than CA and BSA NPs (125.2 *vs* 81.0, 72.4 μm, $P < 0.05$). From the continual *Y*-axis scan layers (10 μm each), it could be seen that the fluorescence signal in M-CA NPs group was more intense and deeper than that in CA and BSA NPs. These findings suggested that CA and BSA NPs have equivalent tumor penetration capacity, while menthol was able to improve intratumoral infiltration of nanoparticles. Therefore, menthol could not only enhance the BBB penetration and the uptake by tumor cells, but also enhance intratumoral infiltration of tumor tissue.

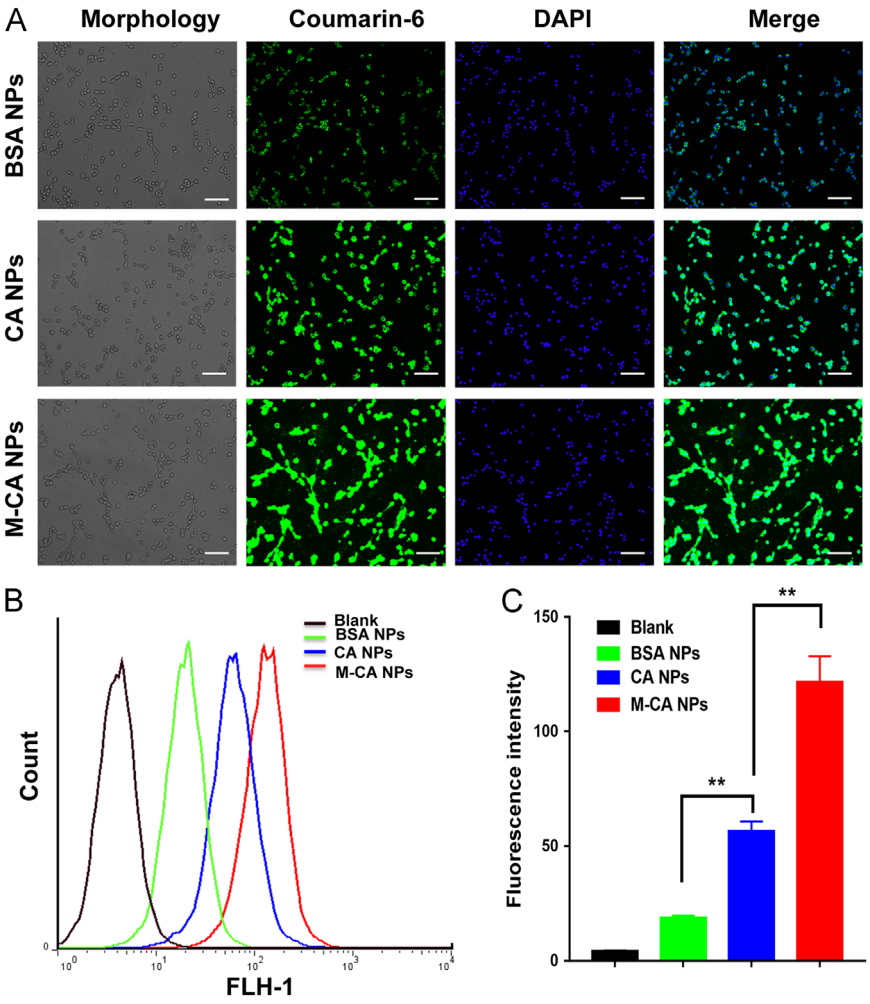

Figure 3 Cellular uptake of nanoparticles at equivalent C6 concentration (50 ng/mL) after incubation for 4 h at 37 °C on C6 cells. (A) Representative fluorescence photomicrographs of C6 cells after treatment with different coumarin-loaded nanoparticles (bar: 100 μm). (B) FACS analysis of uptake and (C) the column chart of the median fluorescence intensity of different nanoparticles groups. Data are represented as mean ± SD, $n = 3$. $^{**}P < 0.05$.

3.6. *In vitro cytotoxicity of NPs*

In vitro cytotoxicity of free HCPT and different HCPT-loaded nanoparticles on C6 cells was measured by MTT assay (Fig. 5 and Table 2). It could be concluded that both free HCPT and HCPT-loaded nanoparticles could inhibit the proliferation of C6 cells in a concentration-dependent manner. Compared with free HCPT (IC_{50} = 0.1078 μg/mL), HCPT-CA-NP (IC_{50} = 0.0603 μg/mL) and HCPT-M-CA-NP (IC_{50} = 0.0397 μg/mL) exhibited greater killing ability and enhanced cytotoxicity on C6 glioma cells. Moreover, HCPT-M-CA-NPs displayed the highest antitumor activity. This should be attributed to the transmembrane capacity of the carrier material casein and the enhanced penetration ability of menthol.

3.7. *In vitro apoptosis assay of NPs*

As shown in Figs. 3A and 6A, the nuclei of untreated C6 cells was spherical and integral with homogenous fluorescence, while the nuclei of the cells treated with different HCPT formulations were severely fragmented, among which HCPT-M-CA-NPs exhibited the most severe fragmentation of the cell nuclei. Annexin V-FITC apoptosis detection kit was used to stain the cells and the cell apoptosis was analyzed by flow cytometry. As shown in Fig. 6B and C, the percentage of early and late apoptosis was significantly increased after the treatment with HCPT, HCPT-CA-NPs and HCPT-M-CA-NPs. Compared with HCPT and HCPT-CA-NPs, HCPT-M-CA-NPs manifested more potent apoptosis response due to higher uptake nanoparticles into tumor cells and produced higher cytotoxicity than HCPT-CA-NP treatment. The effect of HCPT-M-CA-NPs on increasing the total apoptosis of C6 cells was mainly due to the contribution of late apoptosis, which inferred that the HCPT-M-CA-NPs could push forward the transition from early to late apoptosis of C6 cells. Since early apoptosis is reversible and late apoptosis is irreversible, it is beneficial to kill tumor cells through the promotion of late apoptosis or the transition to late apoptosis. The effect was even more obvious when the casein was modified with menthol.

3.8. *In vivo fluorescence imaging of NPs in glioma-bearing mice*

The body distribution of various DiR-loaded nanoparticles in tumor-bearing mice at predetermined time points was shown in Fig. 7A. The order of fluorescence intensity in the brain was M-CA > CA > BSA NPs, indicating that CA NPs are more

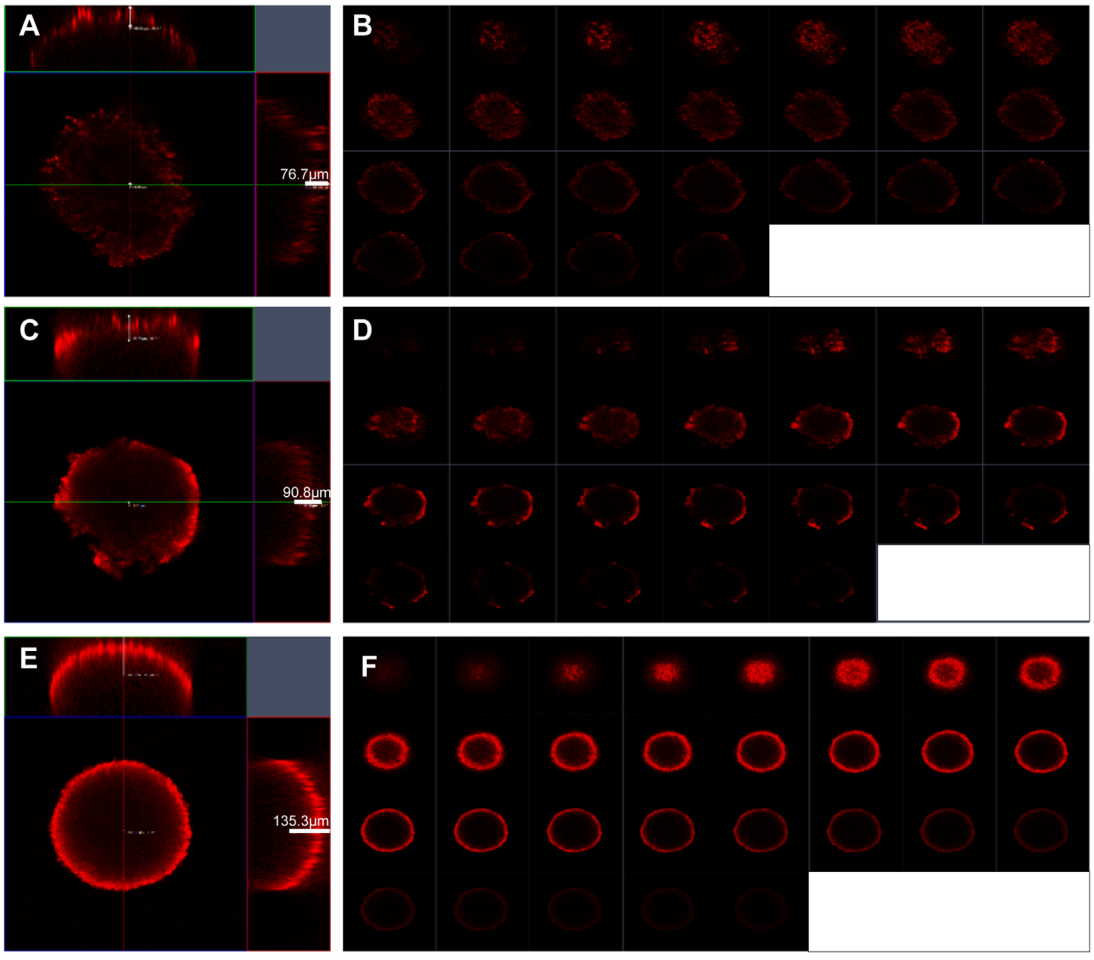

Figure 4 Confocal microscopy analysis of the penetration ability of nanoparticle in 3D tumor spheroids. (A), (C), and (E) show quantitative measurement results of the penetration depth of BSA, CA and M-CA NPs, respectively. (B), (D), and (F) represent multi-level scan of the penetration of BSA, CA and M-CA NPs, respectively. The interval between the consecutive slides was 10 μm.

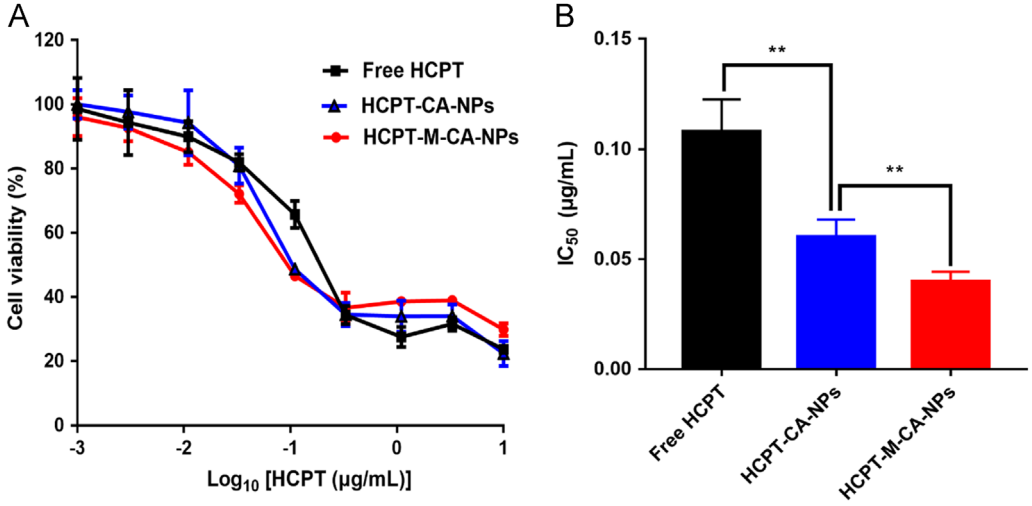

Figure 5 Cytotoxicity of free HCPT and different HCPT nanoparticles against C6 cells 48 h post-incubation at 37 °C (mean ± SD, $n = 6$).

likely to enter the brain than BSA NPs, whereas M-CA NPs are more able to utilize the strong penetration capacity of menthol to be transported into the brain of tumor-bearing mice. Fig. 7B and C captured images of the brain and major organs obtained after cardiac perfusion. Statistical analysis showed that, compared to the BSA NPs group, the distribution of CA and M-CA NPs in the brain was significantly enhanced, which was consistent with the results of the previous cell uptake study. In addition, since the

Table 2 IC_{50} values of free HCPT and different HCPT nanoparticles against C6 tumor cells.

Formulation	IC_{50} (μg/mL)
Free HCPT	0.1078 ± 0.0147
HCPT-CA-NPs	0.0603 ± 0.0079
HCPT-M-CA-NPs	0.0397 ± 0.0045

liver and the spleen are the main organs for metabolism and clearance, the fluorescence intensity of nanoparticle preparations in the liver and spleen is also significantly stronger than other organs.

To further investigate the distribution of DiR-loaded nanoparticles in brain tumor sites of each group, the above brain tissue was cut into 20 μm thick sections and then stained with DAPI. The distribution of DiR in the brain was observed under a laser confocal fluorescence microscope (Zeiss, Jena, Germany). As shown in Fig. 8, tumor tissue cells are denser than normal tissues. In CA and M-CA NPs group, the fluorescence intensity in tumor tissue was significantly stronger than that in normal brain tissue region and the accumulation of nanoparticles in the brain tumor of M-CA NPs was more obvious than that of CA NPs. Whereas, in BSA NPs group, whether the tumor or normal brain tissue, there was no fluorescence signal of DiR, which is consistent with the *ex vivo* image of isolated brain tissue in Fig. 7B. The results on tumor-bearing nude mice demonstrated that casein, as the carrier, and the modification with menthol, could not only enhance the nanoparticles across the BBB, but also improve the accumulative distribution to the tumor site in the brain.

3.9. *In vivo anti-glioma effect of NPs*

To investigate the *in vivo* anti-glioma effect of various nanoparticles, the orthotopic glioma-bearing mice were injected with different HCPT formulations. Fig. 9A showed the body weight changes of every group during the treatment course. A rapid reduction in body weight could be found in the saline group and

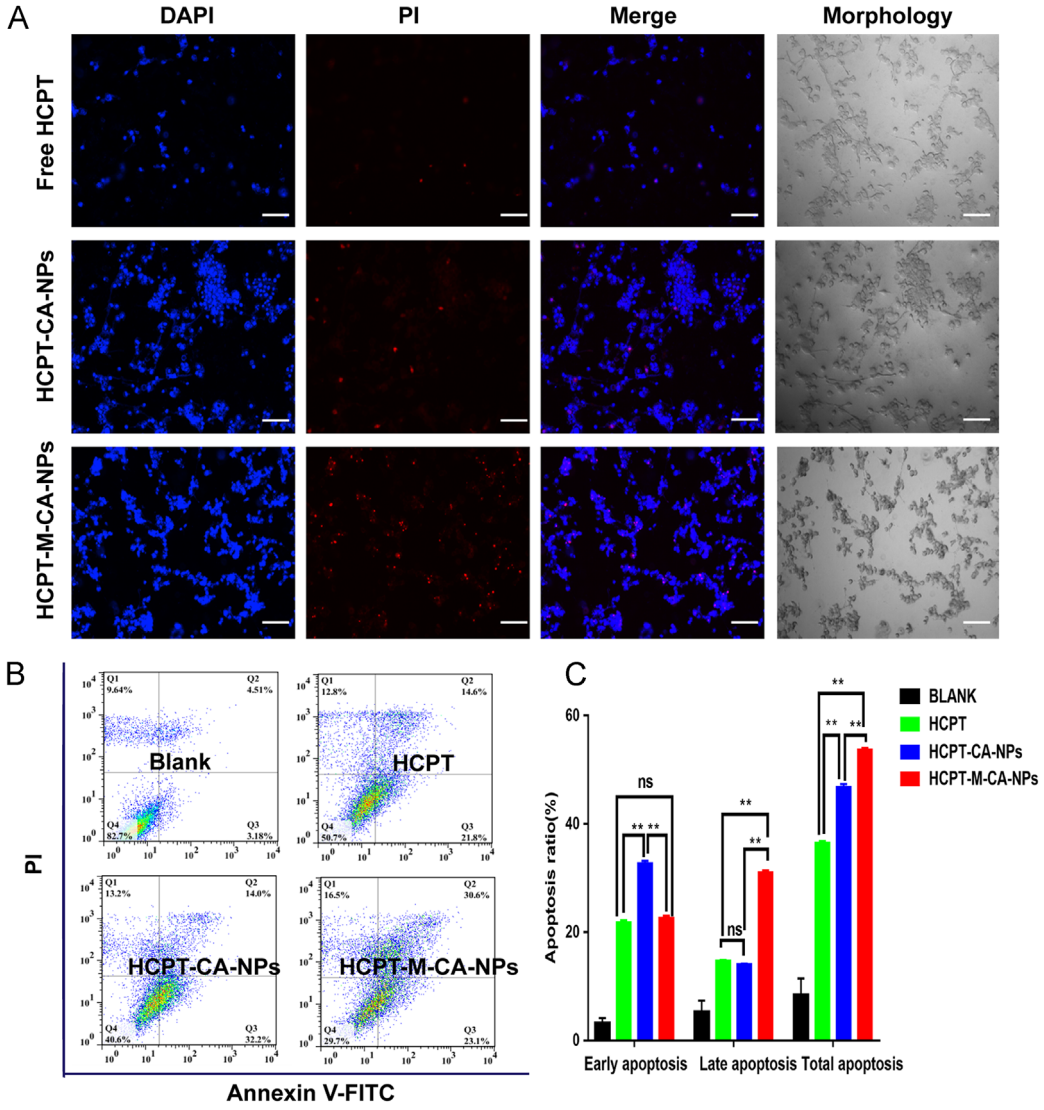

Figure 6 Apoptosis of C6 cells induced by HCPT, HCPT-CA-NPs and HCPT-M-CA-NPs after incubation with equivalent HCPT concentration (312 ng/mL) for 48 h analyzed by fluorescence microscopy (A) and flow cytometry (B) (bar: 100 μm).

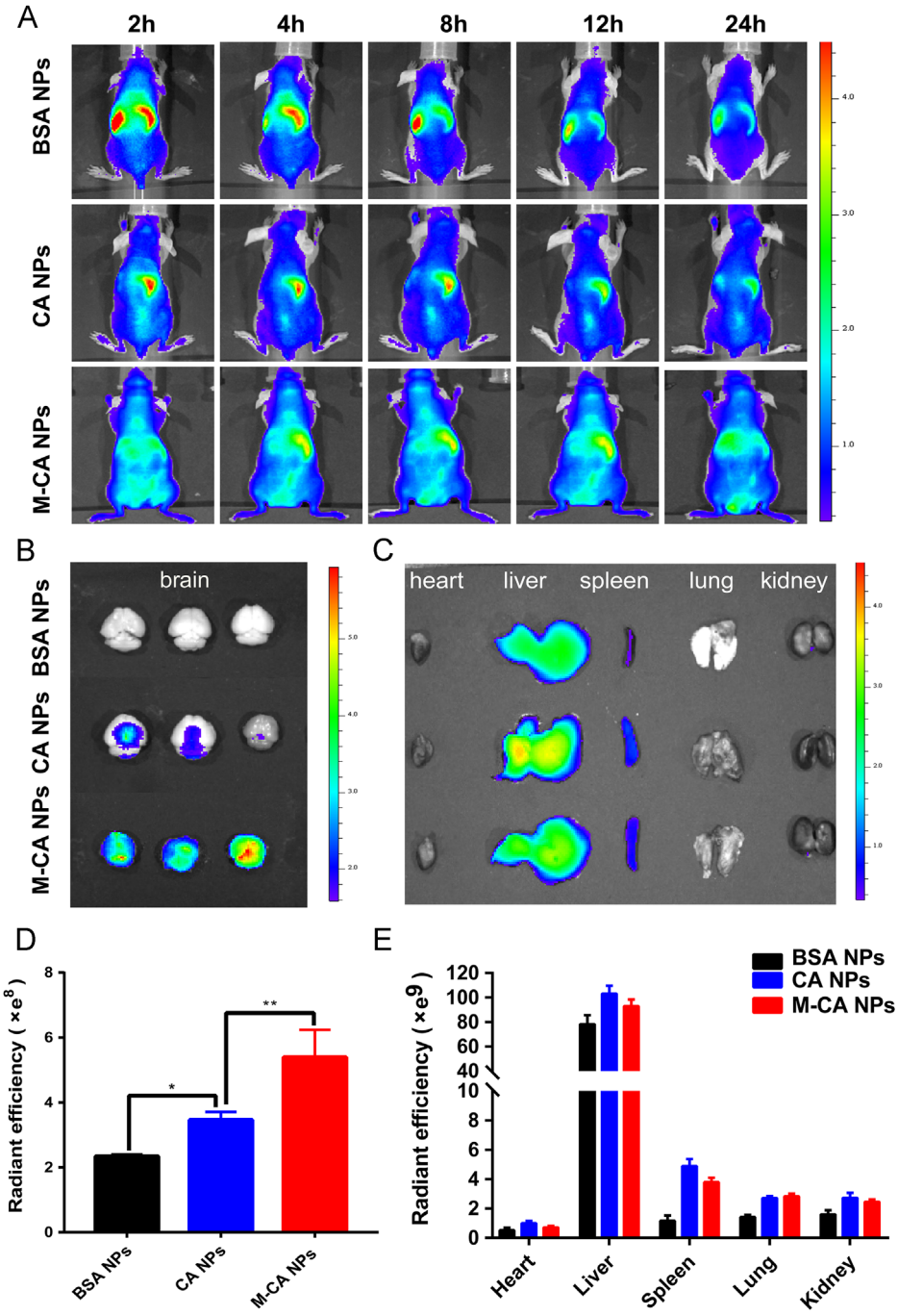

Figure 7 *In vivo* imaging of distribution in mice bearing C6 orthotopic glioma. (A) Whole body imaging of the mice from 1h to 24 h. (B) *Ex vivo* imaging of the brain and (C) the major organs dissected from the mice. (D) *Ex vivo* radiant efficiency of the brain and (E) the main organs Data are expressed as mean ± SD, $n = 3$.

free HCPT group. The body weight decreased slowly in the two groups of nanoparticles, indicating that they could improve the delivery of HCPT into the brain, and increased the ability to resist the rapid growth of glioma to a certain extent. From Fig. 9B, the median survival time of the saline group, HCPT group, HCPT-CA-NPs group and HCPT-M-CA-NPs group was 12.5, 17.0, 22.0 and 25.5 days, respectively. However, all tumor-bearing mice in the saline group died on the Day 14 after inoculation of C6 glioma. This may be due to the higher degree of malignancy of C6 glioma and their rapid growth. The median survival time of M-CA NPs was 2 times of that of the saline group and 1.5 times of that of free HCPT group. There was also a significant difference between the survival time of CA and M-CA NPs. The results showed that HCPT-loaded M-CA NPs could significantly increase the anti-glioma effect and the safety of HCPT.

3.10. *Safety evaluation of NPs*

The main organs (heart, liver, spleen, lung, and kidney) of the mice after anti-glioma experiment were taken, sectioned and HE-stained to observe the pathological changes. As shown in

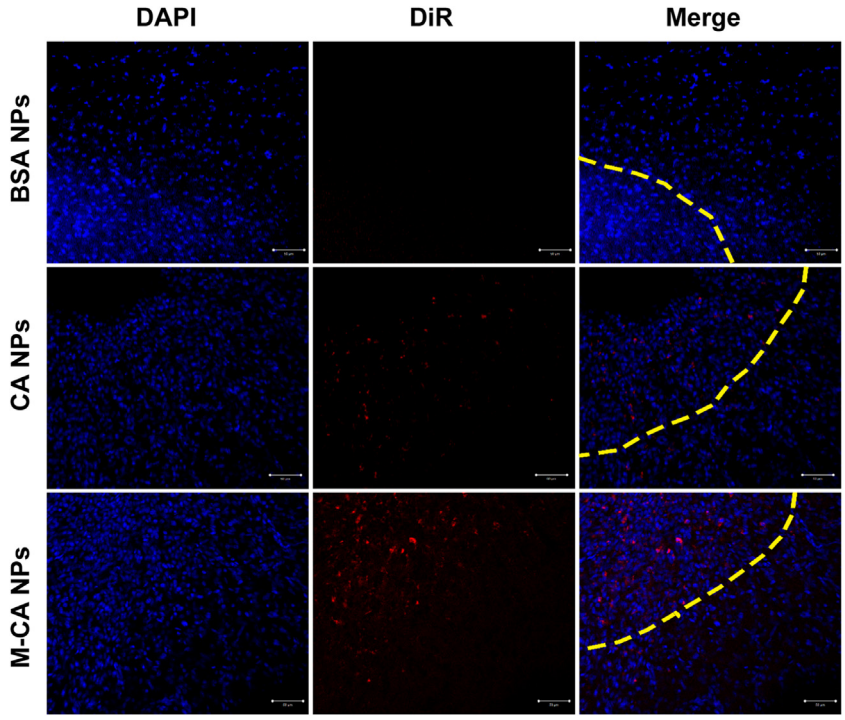

Figure 8 The distribution of DiR in the brain frozen sections after treatment with different DiR-loaded nanoparticles (bar: 50 μm).

Fig. 10, no significant damage was found in all the organs in four groups, implying the good safety of the HCPT, CA NPs and M-CA NPs. According to research reports, the most common clinical adverse reactions of HCPT are gastrointestinal discomfort (nausea, vomiting, etc.), myelosuppression (mainly manifested as a decrease in the level of white blood cells), ECG changes and mild urinary tract irritation symptoms. But these symptoms are not easy to be observed in mice. Casein is used as the main component of milk, and its safety is guaranteed. Research has been conducted on the acute and long-term toxicity of casein in high doses and confirmed that casein is safe[51]. As to menthol-modified casein, since it is very safe and the organic solvent used in the chemical reaction process has been removed by dialysis, no more toxicity was found than CA NPs.

3.11. Binding affinity of casein with LDL receptors and effect on the expression ZO-1 and occludin

The binding assay was conducted to discover the mechanism underlying the enhanced uptake and drug accumulation in the tumor region of CA NPs. Fig. 11 showed that casein could strongly bind with LDL-receptors on the BCEC cells, which might be due to the structure similarity of casein and low-density protein. Moreover, menthol-modified casein exhibit almost the same affinity with LDL-receptor, suggesting the modification of menthol did not affect the binding capacity of casein with LDLR.

According to previous reports, aromatic resuscitation compounds have the ability to open the BBB. So we selected BCEC cell monolayer to investigate the effect of menthol-modified casein nanoparticles on the tight junction protein ZO-1 and occludin expression level. The results in Supporting Information Fig. S2 showed that menthol-modified casein could obviously reduce the expression level of both proteins.

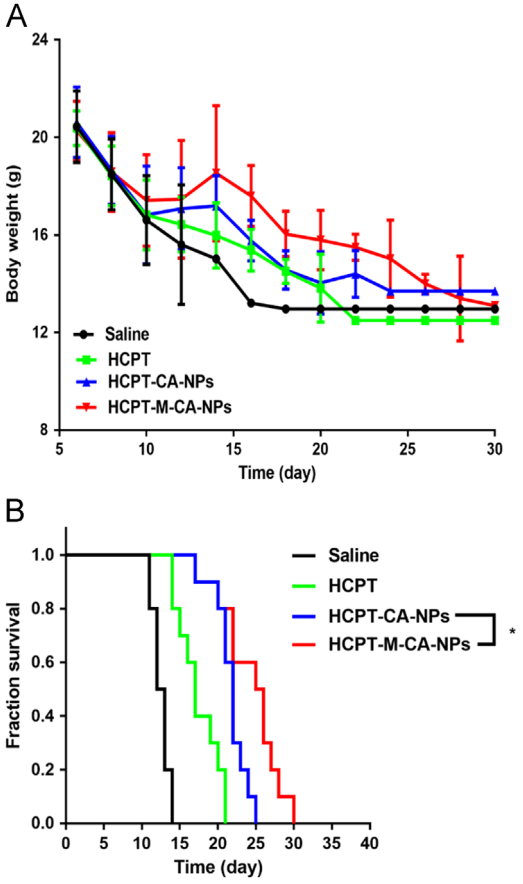

Figure 9 Anti-glioma effect of different HCPT formulations after intravenous administration to intracranial glioma-bearing mice. (A) Body weight change and (B) Kaplan−Meier survival curves of model mice (Data are expressed as mean ± SD, $n = 10$; $P < 0.05$).

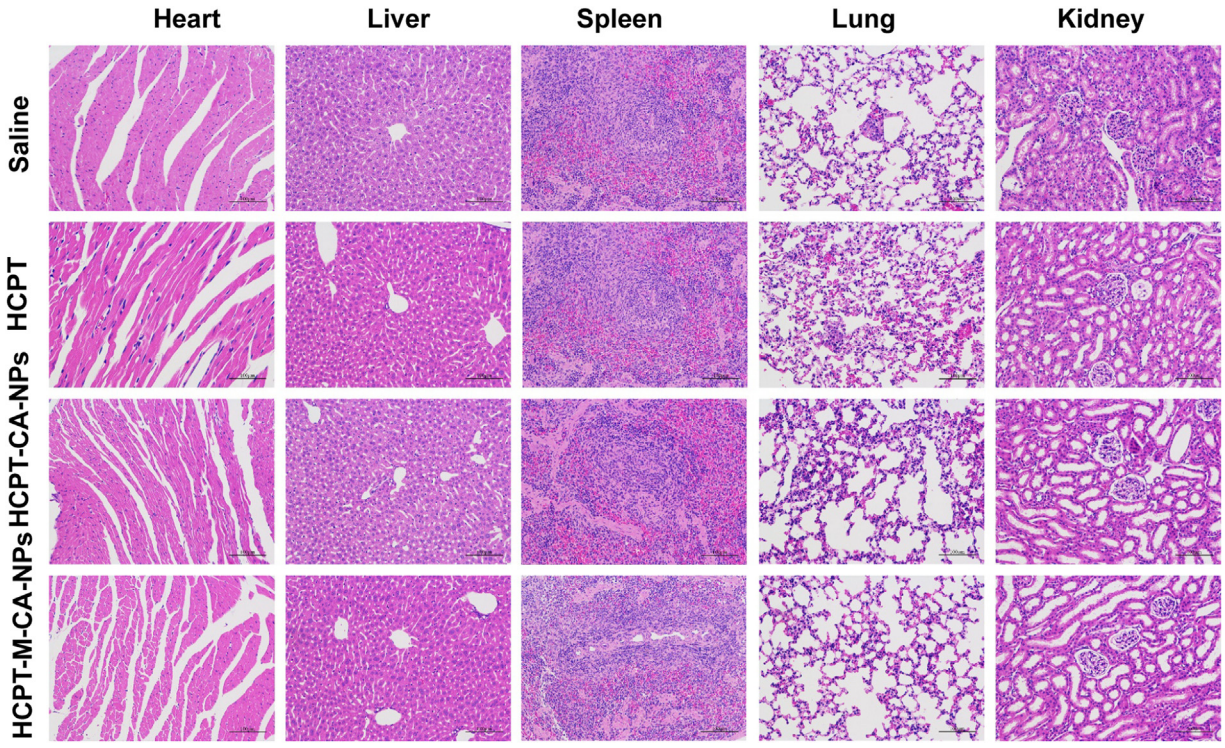

Figure 10 The hematoxylin-eosin staining of the main organ after treatment with different formulations (saline, HCPT, HCPT-CA-NPs and HCPT-M-CA-NPs. Bar: 200 μm).

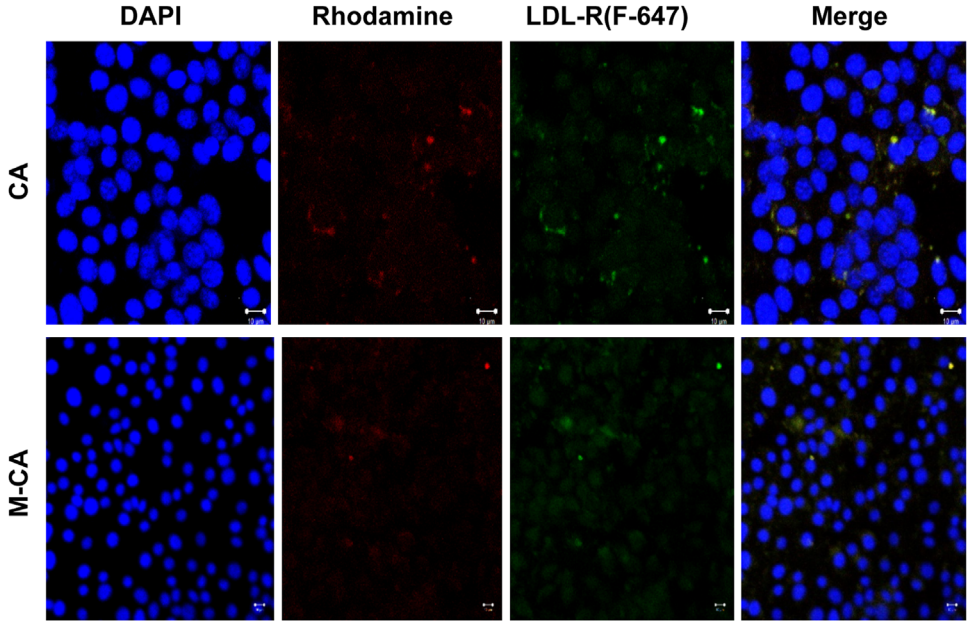

Figure 11 The combination condition of casein and menthol-modified casein after the treatment with rhodamine-labeled casein and menthol-modified casein in BCEC cells (Bar: 10 μm).

4. Conclusions

In this study, we chose a natural compound menthol as a strong brain penetration enhancer and a food protein casein as carrier material, then linked them through chemical covalent method. Subsequently, a menthol modified casein nanoparticle was prepared as a safe and effective chemotherapeutic drug delivery system for the targeting treatment of glioma. This protein-based system exhibited the following features: (i) simple preparation method and good drug loading capacity; (ii) traditional Chinese medicine active ingredient as a target ligand to penetrate through BBB and guide the nanoparticles into the tumor region; (iii) natural and sourceful protein as carrier with excellent and inherent penetration capacity; (iv) low systemic toxicity. The *in vitro* and *in vivo* results indicated that HCPT-M-CA-NPs could enhance the drug accumulation in the tumor region and then prolong the

median survival time of intracranial glioma-bearing mice. Taking together, it could be claimed that menthol modified casein nanoparticles, which combined the advantages of traditional Chinese medicine with modern delivery technology, may serve as a promising platform for the treatment of brain tumor.

Acknowledgments

We are thankful for financial support from the National Natural Science Foundation of China (No. 81573616, 81690263 and 81773911, China) and the Development Project of Shanghai Peak Disciplines-Integrated Medicine (No. 20150407, China). In addition, we also appreciate all people who gave our help and technology instruction in experiments.

Appendix A. Supporting information

Supporting data associated with this article can be found in the online version at https://doi.org/10.1016/j.apsb.2019.01.006.

References

1. Alifieris C, Trafalis DT. Glioblastoma multiforme: pathogenesis and treatment. *Pharmacol Ther* 2015;**152**:63–82.
2. Ostrom QT, Gittleman H, Fulop J, Liu M, Blanda R, Kromer C, et al. CBTRUS statistical report: primary brain and central nervous system tumors diagnosed in the united states in 2008–2012. *Neuro Oncol* 2015;**17**:iv1–62.
3. Serwer LP, James CD. Challenges in drug delivery to tumors of the central nervous system: an overview of pharmacological and surgical considerations. *Adv Drug Deliv Rev* 2012;**64**:590–7.
4. Reni M, Mazza E, Zanon S, Gatta G, Vecht CJ. Central nervous system gliomas. *Crit Rev Oncol/Hematol* 2017;**113**:213–34.
5. Ostrom QT, Gittleman H, Liao P, Vecchione-Koval T, Wolinsky Y, Kruchko C, et al. CBTRUS statistical report: primary brain and other central nervous system tumors diagnosed in the United States in 2010–2014. *Neuro Oncol* 2017;**19 Suppl 5**:1–88.
6. Wahl DR, Lawrence TS. Integrating chemoradiation and molecularly targeted therapy. *Adv Drug Deliv Rev* 2017;**109**:74–83.
7. Anjum K, Shagufta BI, Abbas SQ, Patel S, Khan I, Shah SAA, et al. Current status and future therapeutic perspectives of glioblastoma multiforme (GBM) therapy: a review. *Biomed Pharmacother* 2017;**92**:681–9.
8. Chen Y, Liu L. Modern methods for delivery of drugs across the blood–brain barrier. *Adv Drug Deliv Rev* 2012;**64**:640–65.
9. Zhan C, Lu W. The blood–brain/tumor barriers: challenges and chances for malignant gliomas targeted drug delivery. *Curr Pharm Biotechnol* 2012;**13**:2380–7.
10. Biddlestone-Thorpe L, Marchi N, Guo K, Ghosh C, Janigro D, Valerie K, et al. Nanomaterial-mediated CNS delivery of diagnostic and therapeutic agents. *Adv Drug Deliv Rev* 2012;**64**:605–13.
11. Wong HL, Wu XY, Bendayan R. Nanotechnological advances for the delivery of CNS therapeutics. *Adv Drug Deliv Rev* 2012;**64**:686–700.
12. Byeon HJ, Thao LQ, Lee S, Min SY, Lee ES, Shin BS, et al. Doxorubicin-loaded nanoparticles consisted of cationic- and mannose-modified-albumins for dual-targeting in brain tumors. *J Control Release* 2016;**225**:301–13.
13. Gao H. Progress and perspectives on targeting nanoparticles for brain drug delivery. *Acta Pharm Sin B* 2016;**6**:268–86.
14. Gao H. Perspectives on dual targeting delivery systems for brain tumors. *J Neuroimmune Pharm* 2017;**12**:6–16.
15. Ruan S, Yuan M, Zhang L, Hu G, Chen J, Cun X, et al. Tumor microenvironment sensitive doxorubicin delivery and release to glioma using angiopep-2 decorated gold nanoparticles. *Biomaterials* 2015;**37**:425–35.
16. Bhatia SP, McGinty D, Letizia CS, Api AM. Fragrance material review on menthol. *Food Chem Toxicol* 2008;**46 Suppl 11**: S209–14.
17. Kim SH, Lee S, Piccolo SR, Allen-Brady K, Park EJ, Chun JN, et al. Menthol induces cell-cycle arrest in PC-3 cells by down-regulating G2/M genes, including polo-like kinase 1. *Biochem Biophys Res Commun* 2012;**422**:436–41.
18. Craighead DH, Alexander LM. Topical menthol increases cutaneous blood flow. *Microvasc Res* 2016;**107**:39–45.
19. Brain KR, Green DM, Dykes PJ, Marks R, Bola TS. The role of menthol in skin penetration from topical formulations of ibuprofen 5% *in vivo*. *Skin Pharmacol Physiol* 2005;**19**:17–21.
20. Wang Y, Wang X, Yang Z, Zhu G, Chen D, Meng Z. Menthol inhibits the proliferation and motility of prostate cancer DU145 cells. *Pathol Oncol Res* 2012;**18**:903–10.
21. Lin J, Zhu LQ, Qin T, Yu QH, Yang Q. Enhancement of gene transfer efficiency in the Bcap-37 cell line by dimethyl sulphoxide and menthol. *Mol Med Rep* 2012;**6**:1293–300.
22. Zhang L, Du SY, Lu Y, Liu C, Wu HC, Tian ZH, et al. Puerarin transport across rat nasal epithelial cells and the influence of compatibility with peoniflorin and menthol. *Drug Des Devel Ther* 2017;**11**:2581–93.
23. Yang B, Du S, Lu Y, Jia S, Zhao M, Bai J, et al. Influence of paeoniflorin and menthol on puerarin transport across MDCK and MDCK–MDR1 cells as blood–brain barrier *in vitro* model. *J Pharm Pharmacol* 2018;**70**:349–60.
24. Zhang L, Han L, Qin J, Lu W, Wang J. The use of borneol as an enhancer for targeting aprotinin-conjugated PEG–PLGA nanoparticles to the brain. *Pharm Res* 2013;**30**:2560–72.
25. Ren J, Zou M, Gao P, Wang Y, Cheng G. Tissue distribution of borneol-modified ganciclovir-loaded solid lipid nanoparticles in mice after intravenous administration. *Eur J Pharm Biopharm* 2013;**83**:141–8.
26. Liang J, Gao C, Zhu Y, Ling C, Wang Q, Huang Y, et al. Natural brain penetration enhancer-modified albumin nanoparticles for glioma targeting delivery. *ACS Appl Mater Interfaces* 2018;**10**:30201–13.
27. Wei M. Construction and brain targeting research of solid lipid nanoparticles comodified with borneol and PEG [dissertation]. Beijing: Peking Union Medical College; 2017.
28. Guo J, Gao X, Su L, Xia H, Gu G, Pang Z, et al. Aptamer-functionalized PEG–PLGA nanoparticles for enhanced anti-glioma drug delivery. *Biomaterials* 2011;**32**:8010–20.
29. Hu Q, Gu G, Liu Z, Jiang M, Kang T, Miao D, et al. F3 peptide-functionalized PEG–PLA nanoparticles co-administrated with tLyp-1 peptide for anti-glioma drug delivery. *Biomaterials* 2013;**34**:1135–45.
30. Liu Y, Lu W. Recent advances in brain tumor-targeted nano-drug delivery systems. *Expert Opin Drug Deliv* 2012;**9**:671–86.
31. Xu XL, Li JJ, Han SP, Tao CH, Fang L, Sun Y, et al. A novel doxorubicin loaded folic acid conjugated PAMAM modified with borneol, a nature dual-functional product of reducing PAMAM toxicity and boosting BBB penetration. *Eur J Pharm Sci* 2016;**88**:178–90.
32. Elzoghby AO, Samy WM, Elgindy NA. Protein-based nanocarriers as promising drug and gene delivery systems. *J Control Release* 2012;**161**:38–49.
33. Ruan C, Liu L, Lu Y, Zhang Y, He X, Chen X, et al. Substance P-modified human serum albumin nanoparticles loaded with paclitaxel for targeted therapy of glioma. *Acta Pharm Sin B* 2018;**8**:85–96.
34. Hawkins MJ, Soon-Shiong P, Desai N. Protein nanoparticles as drug carriers in clinical medicine. *Adv Drug Deliv Rev* 2008;**60**:876–85.
35. Sparreboom A, Scripture CD, Trieu V, Williams PJ, De T, Yang A, et al. Comparative preclinical and clinical pharmacokinetics of a cremophor-free, nanoparticle albumin-bound paclitaxel (ABI-007) and paclitaxel formulated in Cremophor (Taxol). *Clin Cancer Res* 2005;**11**:4136–43.
36. Livney YD. Milk proteins as vehicles for bioactives. *Curr Opin Colloid Interface Sci* 2010;**15**:73–83.

37. Elzoghby AO, El-Fotoh WS, Elgindy NA. Casein-based formulations as promising controlled release drug delivery systems. *J Control Release* 2011;**153**:206–16.
38. Pan K, Luo Y, Gan Y, Baek SJ, Zhong Q. pH-driven encapsulation of curcumin in self-assembled casein nanoparticles for enhanced dispersibility and bioactivity. *Soft Matter* 2014;**10**:6820–30.
39. Liu C, Yao W, Zhang L, Qian H, Wu W, Jiang X. Cell-penetrating hollow spheres based on milk protein. *Chem Commun* 2010;**46**:7566–8.
40. Liu C, Zhen X, Wang X, Wu W, Jiang X. Cellular entry fashion of hollow milk protein spheres. *Soft Matter* 2011;**7**:11526.
41. Zhen X, Wang X, Xie C, Wu W, Jiang X. Cellular uptake, antitumor response and tumor penetration of cisplatin-loaded milk protein nanoparticles. *Biomaterials* 2013;**34**:1372–82.
42. Li R, Shu C, Wang W, Wang X, Li H, Xu D, et al. Encapsulation of 10-hydroxy camptothecin in supramolecular hydrogel as an injectable drug delivery system. *J Pharm Sci* 2015;**104**:2266–75.
43. Wu C, Li R, Yin Y, Wang J, Zhang L, Zhong W. Redox-responsive supramolecular hydrogel based on 10-hydroxy camptothecin-peptide covalent conjugates with high loading capacity for drug delivery. *Mater Sci Eng: C* 2017;**76**:196–202.
44. Li G, Cai C, Ren T, Tang X. Development and application of a UPLC–MS/MS method for the pharmacokinetic study of 10-hydroxy camptothecin and hydroxyethyl starch conjugate in rats. *J Pharm Biomed Anal* 2014;**88**:345–53.
45. Bachar M, Mandelbaum A, Portnaya I, Perlstein H, Even-Chen S, Barenholz Y, et al. Development and characterization of a novel drug nanocarrier for oral delivery, based on self-assembled β-casein micelles. *J Control Release* 2012;**160**:164–71.
46. Shapira A, Markman G, Assaraf YG, Livney YD. β-Casein–based nanovehicles for oral delivery of chemotherapeutic drugs: drug–protein interactions and mitoxantrone loading capacity. Nanomed: Nanotechnol. *Biol Med* 2010;**6**:547–55.
47. Liang J, Li R, He Y, Ling C, Wang Q, Huang Y, et al. A novel tumor-targeting treatment strategy uses energy restriction *via* co-delivery of albendazole and nanosilver. *Nano Res* 2018;**11**:4507–23.
48. Al-Abd AM, Aljehani ZK, Gazzaz RW, Fakhri SH, Jabbad AH, Alahdal AM, et al. Pharmacokinetic strategies to improve drug penetration and entrapment within solid tumors. *J Control Release* 2015;**219**:269–77.
49. Zhang B, Sun X, Mei H, Wang Y, Liao Z, Chen J, et al. LDLR-mediated peptide-22-conjugated nanoparticles for dual-targeting therapy of brain glioma. *Biomaterials* 2013;**34**:9171–82.
50. Lin T, Zhao P, Jiang Y, Tang Y, Jin H, Pan Z, et al. Blood–brain-barrier-penetrating albumin nanoparticles for biomimetic drug delivery *via* albumin-binding protein pathways for antiglioma therapy. *ACS Nano* 2016;**10**:9999–10012.
51. Gil AG, Irache JM, Peñuelas I, González Navarro CJ, López De Cerain A. Toxicity and biodistribution of orally administered casein nanoparticles. *Food Chem Toxicol* 2017;**106**:477–86.